Solidification and grain refinement in Ti(48-50)Al2Mn2Nb1B alloys

Liu, Bo; Li, Jing; Hu, Dawei

DOI:
10.1016/j.intermet.2018.07.018

Document Version
Peer reviewed version

Citation for published version (Harvard):
Liu, B, Li, J & Hu, D 2018, 'Solidification and grain refinement in Ti(48-50)Al2Mn2Nb1B alloys', *Intermetallics*, vol. 101, pp. 99-107. https://doi.org/10.1016/j.intermet.2018.07.018

Solidification and grain refinement in Ti(48-50)Al2Mn2Nb1B alloys

Bo Liu, Jing Li and Dawei Hu[1]

School of Metallurgy and Materials, University of Birmingham,

Edgbaston, Birmingham B15 2TT, UK

Abstract

Two TiAl-based alloys, Ti48Al2Mn2Nb1B and Ti50Al2Mn2Nb1B, were prepared via conventional ingot melting and unidirectional solidification (Bridgman process) to investigate their solidification behaviour and the effect of boron addition on grain refinement. Both of them are found to be α solidifying alloys. Their microstructures are refined, featuring fine and randomly oriented lamellar colonies about 150μm in size, in conventional ingots but the unidirectionally solidified alloys still have columnar microstructures. The entirely different grain refinement behaviour in ingots and Bridgman samples gave rise to the notion that the enhanced α nucleation from the liquid is the key to grain refinement in the two α solidifying alloys although the specific mechanisms are yet to identify.

Keywords: Titanium Aluminide; TiAl; Solidification; Microstructure; Grain refinement; Boron.

1. Introduction

The successful insertion of titanium aluminides blades into low pressure turbines (LPT) in commercial aeroengines by General Electric and Pratt & Whitney in the past few years heralded the era of fruition of titanium aluminides research and development starting about forty years ago[1,2]. The application of light weight titanium aluminides in aeroengines enables great fuel saving and low impact to the environment by increasing fuel efficiency and reducing exhaust gases. Of the TiAl LPT blades for the two commercial aeroengines, GEnx and PW1100G, the large ones (GEnx) were manufactured using investment casting technology and the relatively small ones (PW1100G) were produced through forging. Investment casting is a well-established processing technology with a relatively low cost, especially for large sized low pressure turbine blades. However, the as-cast microstructures of many titanium aluminide alloys feature very large gains (or lamellar colonies in another term). Large grains leads to low tensile ductility and large property scatters. In order to maintain certain ductility and high property repeatability of components refined

[1] Corresponding author. *Email address:* d.hu@bham.ac.uk (D. Hu).

grains/lamellar colonies are essential[3]. To achieve fine grains in cast Ti48Al2Cr2Nb low pressure turbine blades great efforts have been put into developing and improving heat treatment schemes consisting of multi steps of solution treatments and hot isostatic pressing (HIPping) by GE[4,5]. Such activities were also succeeded by Safran S.A. later to develop a simplified heat treatment scheme for their cast semi-products of Ti48Al2Cr2Nb blades[6]. Despite the removal of HIPping the improved heat treatment scheme still takes a long time. Hence it is desirable to have fine microstructures in as-solidified TiAl alloys for being cost-effective and boron addition has been shown to serve the purpose. The practice of adding boron into TiAl alloys to refine as-solidified microstructures stretches back to the debut of Ti45Al2Mn2Nb(XD) around 1990 and TiAl alloys containing boron have been intensively studies since then[7,8]. Ti45Al2Mn2Nb1B has been investigated for cast LPT blade application and only a simple HIPping+ageing combination is needed after casting. Boron addition even is used to help refine the grain size in the latest wrought beta-solidifying TNM alloys[9].

Alongside technological advance in manufacturing aero-engine components the demand for scientific understanding into grain refinement mechanisms has been increased and so have been the research activities in this field. The dedicated and unambiguously evidenced research relating grain refinement to alloys' solidification pathways was first published in 2007 and has been continued even since[10-12]. The findings so far are summarised here. The most studied TiAl alloys have aluminium concentrations ranging from 43 to 52% (atomic percentage is used throughout, unless otherwise stated). At the low aluminium end the alloys solidify via the beta phase ($L \rightarrow \beta$), and at the high Al end via the alpha phase ($L \rightarrow \alpha$). In between a peritectic reaction, $L + \beta \rightarrow \alpha$, occurs. The extent of the peritectic reaction is dependent on Al concentration and with increasing Al the peritectic reaction is reduced in terms of the involved β phase volume. Whether the primary solidification phase is borides or metallic phases depends upon boron concentration in TiAl-B alloys. The dividing value lies approximately at 1%B, being slightly reduced with increasing Al. Below it alloys solidify via metallic β or α phase and titanium boride is the primary solidification phase when boron concentration is high, which can be seen from the measured or/and simulated phase diagrams [13,14].

Alloys with high boron concentration has long been studied. For example, the Ti45Al2Mn2Nb(XD) was derived from TiAl-TiB_2(XD) composites by reducing boron concentration from 7% to 1%[7]. Nonetheless only recently has the grain refinement mechanism in high B-containing alloys been seriously investigated by Gosslar et al although a hypothesis of boride inoculation was mentioned for the XD composites much earlier[15,7]. Gosslar et al found that in Ti45Al2B it was the heterogeneous nucleation of the β phase by primary titanium boride particles in the liquid metal that led to grain refinement[15]. It was also hinted, though no direct evidence was presented, that such heterogeneous nucleation could occur to the α phase in α solidifying alloys.

For most studied alloys the boron concentration is at 1% or below and in those alloys the primary solidification phase is β or α. In the alloys of this category, grain refinement is closely related to solid β phase in the fully beta solidifying alloys and the alloys with

significant extent of peritectic reaction. Grain refinement in beta solidifying alloys has been well documented and the refinement was achieved during $\beta \rightarrow \alpha$ solid phase transformation rather than the solidification[10,16]. It is the already existing boride precipitates that stimulate α phase nucleation during solid phase transformation, enabling all the possible Burgers α variants, to achieve fine α grains, giving rise to fine lamellar colonies in subsequent $\alpha \rightarrow \gamma$ phase transformation. The critical boron concentration is very low and 0.1% is enough for some high-Nb containing alloys. In alloys with higher B concentrations, up to 1%, the excessive boron forms boride particles from the liquid in the interdendritic areas, leading to formation of non-Burgers α during $\beta \rightarrow \alpha$ solid phase transformation[16-18].

The TiAl alloys with a peritectic reaction at about 1490°C can be separated into two groups: hypo-peritectic and hyper-peritectic. The first has a peritectic reaction of $L + \beta \rightarrow \alpha$ and the liquid was completely consumed before the β phase during the reaction under equilibrium conditions. In the second group the liquid is in excess and some is left to solidify as the γ phase after β being exhausted. According to the phase diagram proposed by Witusiewicz et al the Al concentration separating the two groups is 47.6% in Ti-Al binary systems[14]. The grain refinement in the alloys of the first group was found to start in the interdendritic regions but close to the β dendrites by precipitating peritectic α grains inoculated by existing boride particles in the liquid. The peritectic α grains have defined orientation relationship with the inoculating boride particles, and grow into the surrounding β dendrites, consuming both liquid and the β dendrites[11]. Owing to the randomness in orientation of the inoculating boride particles most α grains are also randomly oriented. The critical boron concentration for grain refinement, in this case, can be understood as the minimum amount of boron to form boride particles in the interdendritic liquid prior to the peritectic reaction.

As to the hyper-peritectic alloys, i.e. 47.6%<Al<49.4%, there are no published work regarding their grain refinement mechanisms. Also no such work has been reported in α solidifying TiAl alloys to date. The purpose of this paper is to report our latest work on TiAl-1B with Al of 48-50% solidifying with limited peritectic reaction or alpha phase, in order to complete the spectrum of grain refinement mechanism in TiAl-B in the most studied Al and B ranges.

2. Experimental

The alloys used in this study were Ti48Al2Mn2Nb1B and Ti50Al2Mn2Nb1B. The alloying was to keep it consistent with previous work on Ti45Al2Mn2Nb1B, a well-studied alloy. They were prepared via cold hearth plasma arc melting in the form of 1kg hemispherical buttons. The buttons were melted four times with turning about 90° each time before the next melting to improve homogeneity. Blocks weighing 20g were taken from the buttons and remelted into finger-shaped ingots using non-consumable electrode arc melting in a water cooled copper crucible in Ar atmosphere and the ingots were melted twice and turned over

after the first melting. The remelting was carried out under the same conditions for the two alloys to ensure the same/similar thermal history of them. The aluminium concentration of the finger ingots were measured using energy-dispersive X-ray spectroscopy (EDX) in a scanning electron microscopy (SEM), being 48.0% and 49.9% respectively which were calibrated with a Ti45Al2Mn2Nb standard sample.

Cylinders with 8mm in diameter were also taken from the buttons as the feedstock for preparing Bridgman specimens. The samples were prepared using the Bridgman-Stockbarger technique in ACCESS Materials and Processes at a constant growth rate V of $8.33x10^{-5}$ ms^{-1} and a constant temperature gradient in liquid at the solid-liquid interface G_L of $2\ x10^4$ Km^{-1}. Crucible tubes made of densely sintered yttria were used to minimise oxygen pickup during experiment. The furnace operates under 1000 mbar Argon. Solidification process was frozen by liquid metal quenching with a cooling rate of about $100°Cs^{-1}$. Detailed description of this equipment and process can be found in Refs 16 & 19.

Samples for microstructural assessment were mounted into conductive Bakelite and ground successively to grit 1200 grinding paper. They were mechanically polished using 0.3μm alumina suspension to finish. The as-polished samples were examined using SEM in back-scattered electron (BSE) mode and using electron backscatter diffraction (EBSD) with an INCA software.

3. Results

3.1 Microstructures and orientation analysis of 20g-finger ingots

The 20g-finger ingots cooled down fairly fast during solidification owing to their small volume. It was noted that the temperature dropped 600°C after 1 minute from power off and the cooling rate during solidification was estimated as at the order of $1°Cs^{-1}$ considering the fact that cooling rate is normally high at high temperature and drops with cooling. Observation was made in areas away from the surface, especially regions in contact with the crucible to avoid the chilling effect.

3.1.1 Ti50Al2Mn2Nb1B

According to phase diagrams Ti50Al2Mn2Nb1B should solidify via the α phase since the low alloying additions will not alter the phase diagram much. Figure 1 shows a BSE SEM image of the ingot. The microstructure is consisted of lamellar colonies, the γ-TiAl grains with dark contrast (arrowed) and some fine rod-like TiB_2 precipitates (arrowed) also in dark contrast. The lamellar colony boundaries are delineated by white dashed lines according to their lamellar interface orientation. The lamellar colonies have a few important features which could help understand the solidification process. Firstly, they are almost equiaxed with an average size of about 150μm determined using linear intercept method, in contrast to the columnar structure often found in boron-free alloys, indicating grain refinement. Secondly, each colony contains one or more dendrites but it was not found that a same dendrite is

shared by different lamellar colonies. Thirdly, the dendrites have a hexagonal morphology and the angles between the secondary dendritic arms in the colonies marked with 'A' are almost 60°. The two lamellar colonies are such oriented that their lamellar interface are nearly parallel to the image plane, i.e. the *c*-axis of the α_2 phase is almost parallel to the image normal, which is manifested by their very wide apparent lamellar spacing. Thus, it is clear that this alloy solidified via the α phase. The solidification is expressed as $L \rightarrow \alpha + L$, and the remnant liquid solidified as γ grains between α dendrites and between secondary dendritic arms, as can be seen in the image where many of them are located along the white dashed lines. Fine TiB_2 particles, with dark contrast and in rod-like forms, can be found throughout the alloy matrix. They are distributed very evenly, not segregating into interdendritic areas. The boride particles within the same dendrite still have different orientations, suggesting that they should have formed in liquid before the dendrites.

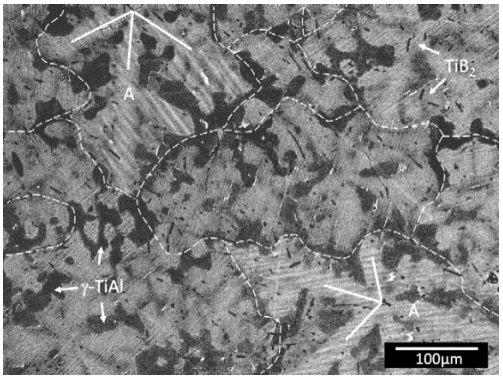

Figure 1 SEM BSE image of Ti50Al2Mn2Nb1B 20g ingot.

The orientation of the microstructural features was analysed using EBSD. Figure 2a shows an analysed area in SEM BSE mode and its Normal-orientation map is given in Fig.2b. The lamellar colony boundaries are marked by white lines in the orientation map. The lamellar interface normal direction, i.e. the *c*-axis of the α_2 phase, in each lamellar colony is shown in the pole figure in Fig.2c. The lamellar orientation is quite random. Detailed analysis did not reveal any orientation relationship between them and it can be said that the α dendrites (the precursors of the lamellar colonies) are very likely to have formed independently to each other in the melt. The lamellar colony no.1 has its lamellar interface normal very close to the N direction (the centre) of the pole figure, which is consistent to its wide apparent lamellar spacing shown in the upper-left of the BSE image. As the last solidifying constituent the γ phase is expected to nucleate on the existing α dendrites and would, as a consequence, have orientation relationships with abutting α dendrites. This has been proven true by orientation analysis. The γ grains, in Fig.2a, having OR with lamellar colonies were assigned the numbers of their orientation counterpart lamellar colonies. Figure 3 shows the {111} pole figures of lamellar colony no.13 and one of the no.13 γ grains. Clearly, this γ grain has the same orientation as one γ variant in that lamellar colony. It should have nucleated on the α dendrite in the final step of solidification. There are a few γ grains marked with 'X's and no OR was found between them and their surrounding lamellar colonies. Nevertheless, there is still a possibility that they could have OR with lamellar colonies above or below the image plane.

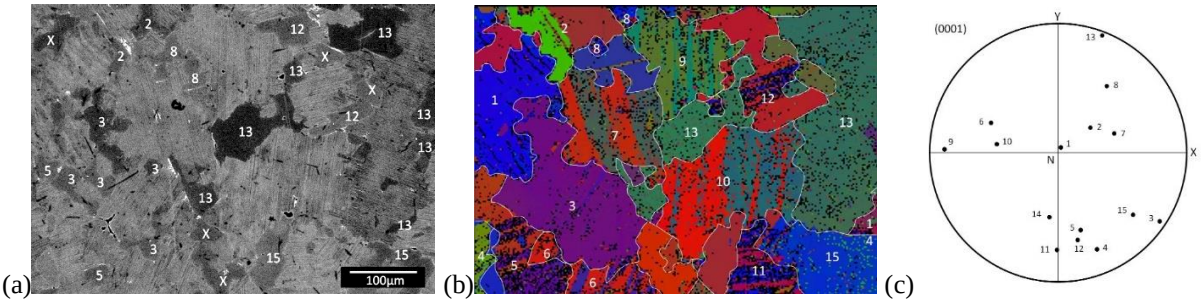

Figure 2 Orientation of the lamellar colonies and γ grains in Ti50Al2Mn2Nb1B 20-g ingot. (a) SEM BSE image, (b) EBSD orientation map and (c) pole figure of lamellar interface normal.

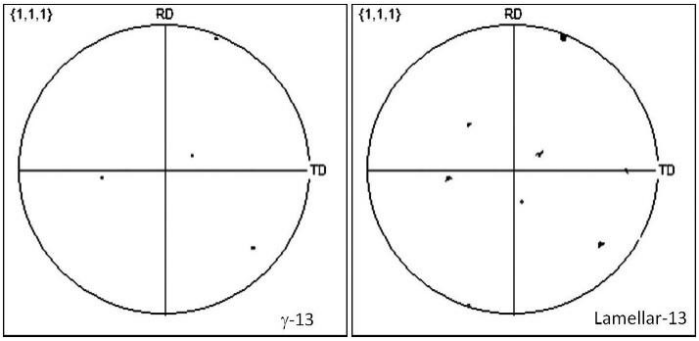

Figure 3 Pole figures showing the orientation relationship between γ grain 13 and lamellar colony 13 in Ti50Al2Mn2Nb1B ingot.

3.1.2 Ti48Al2Mn2Nb1B

The microstructure of as-solidified Ti48Al2Mn2Nb1B ingot is shown in Fig.4a. It has almost equiaxed refined lamellar colonies of which the boundaries are delineated according to lamellar orientation. The lamellar colony size is quite heterogeneous with an average value of about 130μm. TiB_2 particles, with a dark contrast, appear to tend to segregate into interdendritic area (Fig4b). Again, the lamellar colony boundaries are primarily between α dendrites. As in the 50Al alloy the lamellar colonies in this alloy are also α dendrite-based. The interdendritic areas are rich in Al, as suggested by the darker contrast of the BSE image, and there are a small number of γ grains, as shown in Fig.4b, formed directly from the last liquid phase.

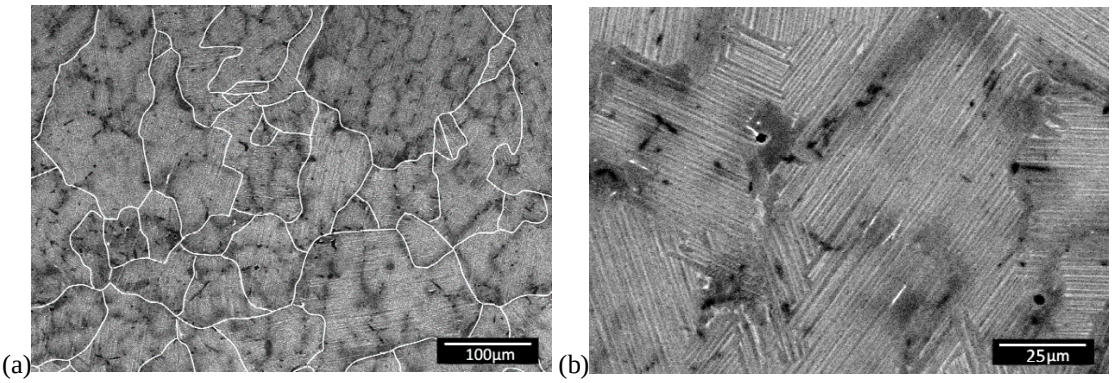

Figure 4 (a) SEM BSE image showing the as-cast microstructure in Ti48Al2Mn2Nb1B 20g ingot with the white lines delineating lamellar boundaries. (b) View at a high magnification.

EBSD was carried out to characterise the orientations of the lamellar colonies. The selected area and its N-orientation map are shown in Fig.5a & 5b. The pole figure in 5c shows the lamellar interface normal (the *c*-axis of the α_2) orientation of the colonies. The angles between their lamellar interface normal were calculated and the 60°-pairs are 1-4 (57.7°), 1-5 (61.3°), 2-3 (58.7°), 2-4 (61.6°) and 4-6 (59.7°), allowing an error within 3°. Also the angle between colonies 2 and 6 is 1.9°, nearly parallel to each other. It is well known that the angle between the *c*-axes of any Burgers α grains can only be 0°, 60° or 90°. Thus by examining the orientation relationship between the α grains whether they are Burgers α variant-related can be ascertained. The method used here was described in details in an earlier work[11] and it is to measure the angles between the *a*-axes of two α grains and compare them to the theoretical values. The orientation of the *a*-axes of each parent α grain can be obtained from the $\{110\}_\gamma$ pole figure of the lamellar colony. The three coincide {110} poles from matrix γ variants and twinning γ variants are the orientations of the *a*-axes. Figure 6 shows the *a*-axes poles (circled) of lamellar colonies 2 and 6 and it can be see there is an rotation of ~12° about the *c*-axes 2 and 6 in Fig.5c, being very close to the theoretic rotation of 10.5°. Thus, this pair has a possibility to be Burgers α variant-related. The rest have been confirmed to have no Burgers α variant relationship between them. The observation of possible Burgers α variants is not a prominent feature in view of its rarity and it is not a sufficient support to the possibility of a β parent phase prior to the α grains.

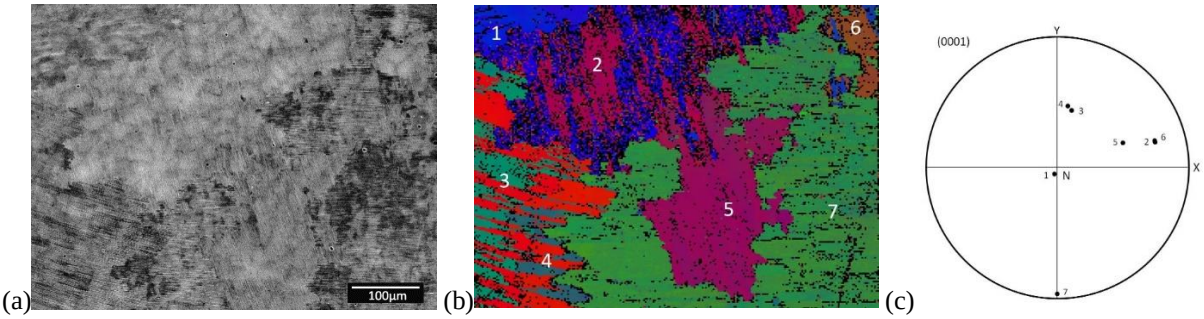

Figure 5 (a) BSE image of an area of Ti48Al2Mn2Nb1B ingot. (b) EBSD orientation map and (c) pole figure showing the lamellar normal orientation of the colonies.

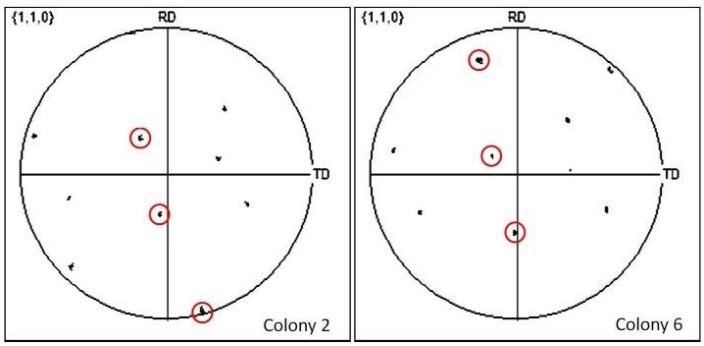

Figure 6 Pole figures showing the orientation relationship between lamellar colonies 2 and 6 in Ti48Al2Mn2Nb1B ingot.

3.2 Microstructures and orientation analysis of Bridgman samples

The preparation of Ti50Al2Mn2Nb1B Bridgman sample was not successful due to gas bubble formation in the sample. The section containing liquid broke up during quenching and the part containing mushy zone was missing. The rest is shown in Fig. 7 and only the solidified section was used for analysis in this study. The Ti48Al2Mn2Nb1B sample was successfully prepared and the different sections are labelled as liquid (L), liquid+solid (L+S), solid (S) and unmelted (U).

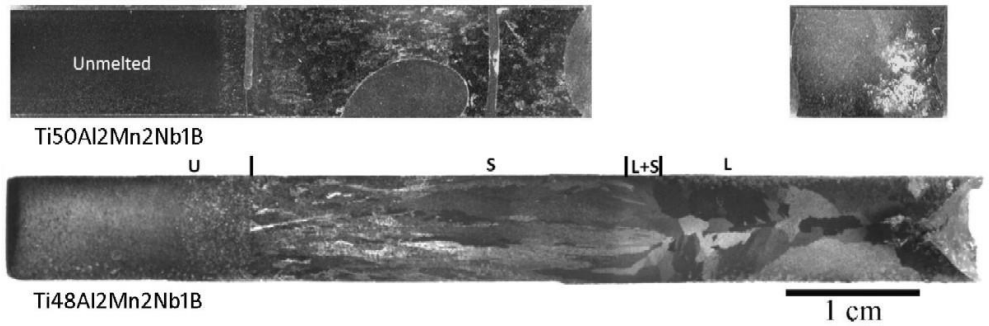

Figure 7 Macrostructures of Ti48Al2Mn2Nb1B and Ti50Al2Mn2Nb1B Bridgman samples.

3.2.1. Ti50Al2Mn2Nb1B

Although the macrostructure of the as-solidified Ti50Al2Mn2Nb1B in the middle section of the Bridgman sample appears lack of typical columnar features, its microstructure still shows elongated lamellar colonies along the solidification direction. Figure 8 is a montage of BSE images in the solidified section. The lamellar colony boundaries are highlighted using white lines and the dashed lines denote the lamellar interface trace. The white arrow indicates the solidification direction. Some γ grains with a dark contrast are located mainly along the lamellar colony boundaries. The lamellar interface traces have angles 45-90° to the growth direction, which is resulted from α dendrite growth deviating from the *c*-axis. What is obvious is that the lamellar colonies are very large and not refined, in contrast to what was observed in the finger ingot.

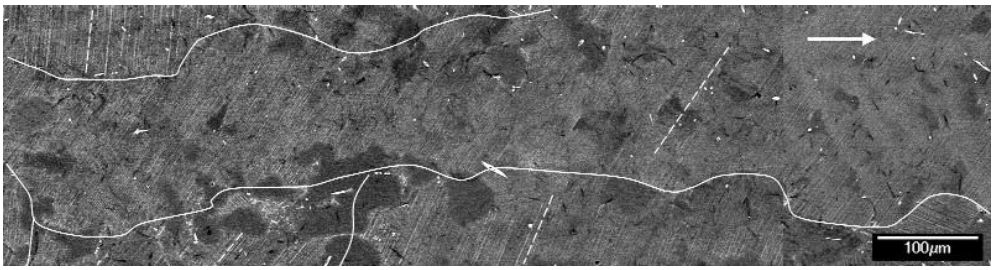

Figure 8 Montage of BSE images showing the microstructure in solidified section of Ti50Al2Mn2Nb1B Bridgman sample. Arrow is the solidification direction. Solid lines mark the lamellar boundaries and dashed straight lines show the lamellar interface traces.

3.2.2. Ti48Al2Mn2Nb1B

The Bridgman sample of Ti48Al2Mn2Nb1B has typical macrostructures through its length. Starting from the left is the unmelted section, a columnar section is in the middle and an equiaxed section to the right in Fig.7. The equiaxed grain structure was formed during quenching at the end of sample preparation. The solidification front is in the (L+S) region between the columnar and equiaxed grain sections. Apparently the grain size was not refined during the directional solidification process.

The microstructural characteristics of the liquid+solid (L+S) region, i.e. the mushy zone, and the solid (S) region are revealed in the BSE image montages in Fig.9. The solidification direction is from left to right, indicated by the white arrows. There are fine dendrites with well-developed secondary arms in the L+S region (Fig.9a) together with titanium boride precipitates which are long and have their longitudinal direction roughly aligned with the dendrites' growth direction. The coarse boride precipitates are located both inside the dendrites and in the interdendritic areas. Such boride precipitates were formed from the liquid metal during unidirectional solidification (before final quenching). The vertical dashed white line indicates the boundary position where all long coarse boride precipitates were found to its left in this image. The boride precipitate shown in the insert is the one at the middle of the dashed line. This position is very close to the tips of the dendrites, slightly behind the solidification front. There are also some white particles in different shapes and they are yttria particles formed through the reaction between liquid metal and the crucible, which has been frequently observed in Bridgman TiAl samples [20]. The microstructure in the solidified region is shown in Fig.9b which contains sections of two lamellar colonies with their boundary delineated. The colonies are elongated in the solidification direction and each of them contains a few parallel dendrites. The lamellar interface traces lie at angles, about 60° to the growth direction. The growth direction of the α dendrites deviated away from the *c*-axis. The long boride precipitates are roughly aligned with the dendrite growth direction.

The dendrites in the mushy zone have actually transformed into lamellar colonies during cooling, but the lamellar interface traces cannot be resolved in Fig.9a owing to the low magnification of the image. Figure 10a shows a high magnification image of a dendrite in this region, showing unambiguously the lamellar interface traces across the dendrite at an angle of about 55°. This dendrite grew from left to right and is in the solidification direction. The pole figure obtained using EBSD in Fig.10b shows the crystalline axes of the parent α dendrite. The X-axis in the pole figure is the solidification direction and parallel to the solidification direction. There is a marked deviation of c-axis from the solidification direction.

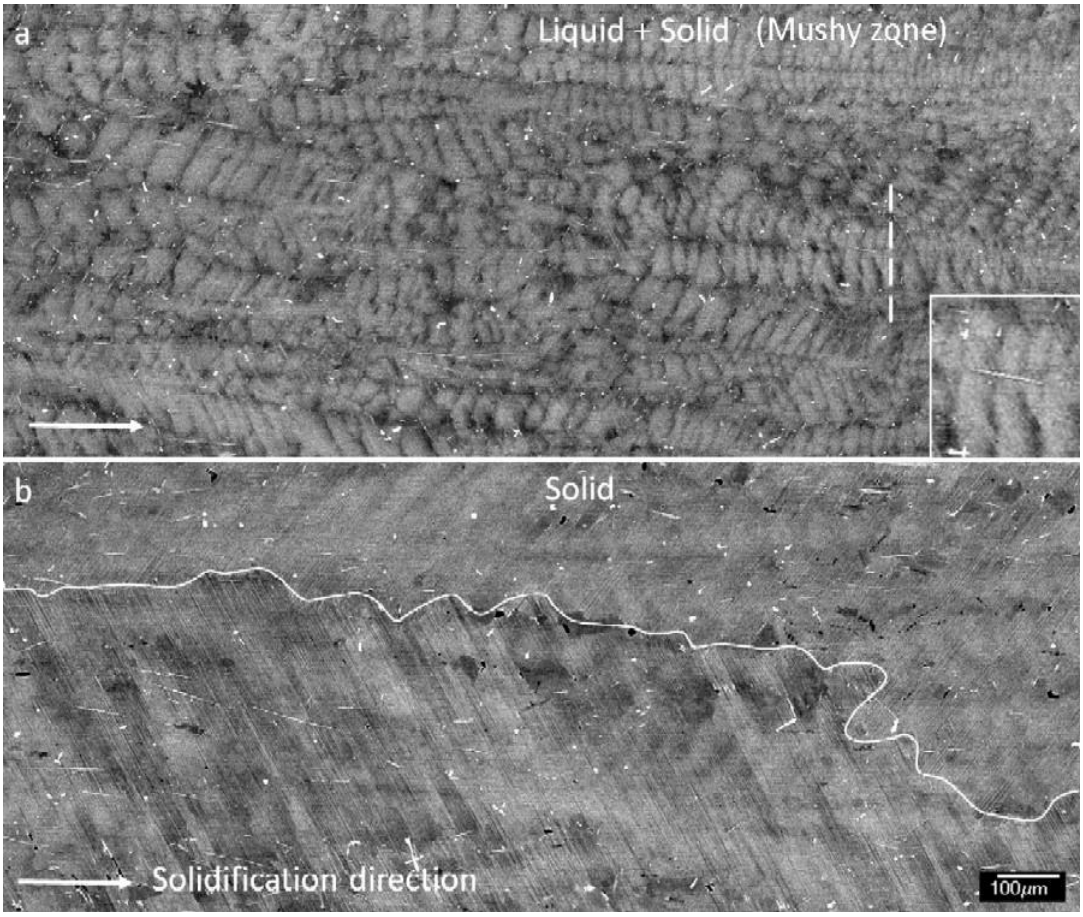

Figure 9 Montages of BSE images showing the microstructures in (a) L+S region (Mushy zone) and (b) solidified region of the Ti48Al2Mn2Nb1B Bridgman sample. The magnification of the insert in (a) is two times of the original image's.

(a)

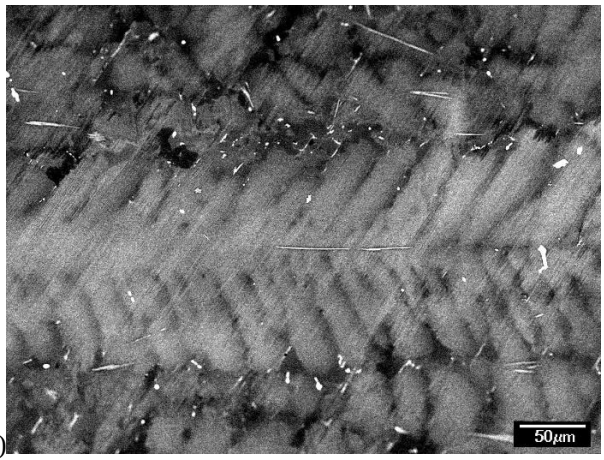

(b)

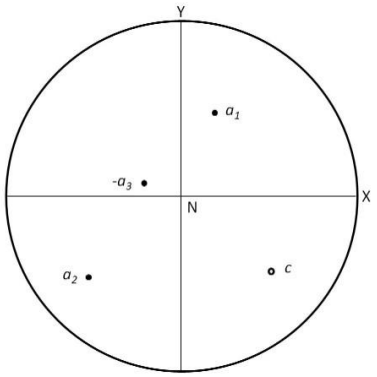

Figure 10 (a) BSE image of a dendrite in the L+S region of the Ti48Al2Mn2Nb1B Bridgman sample. The solidification direction is to the right. (b) The pole figure showing the hcp crystalline axes of the dendrite.

To measure the dendrite growth crystalline direction a cross section in the L+S region was analysed using EBSD. Figure 11a shows the microstructure of an area, and the lamellar colony boundaries are marked according to their orientations for clarity. This area contains 8

lamellar colonies and the *c*-axes of their parent α dendrites are shown as the black closed dots in the pole figure in Fig.11b. It can be seen that none of them is parallel to the N-direction (the solidification direction). For statistical purpose more areas on the same cross section were analysed and the results are superimposed onto this pole figure. Still, none of them is parallel to N. A circle at 40° from N encloses most of the poles. The specific dendrite growth crystalline direction of each α dendrite was calculated and is given in the hcp-α stereograph in Fig.11c. It seems that the dendrite growth crystalline direction lies in a belt 20-40° from the *c*-axis. It should be borne in mind that the method of converting the (0001) pole figure into α stereograph contains an implicit assumption which is that the dendrite growth direction is parallel to the solidification direction. Apparently it is not always true since some dendrites grew slightly off the solidification direction as can be seen in Fig.9a. Such an off-alignment could contribute to the error in the obtained dendrite growth crystalline directions which would cause the results to be shown as a scattered belt in Fig.11c rather than a few discrete points.

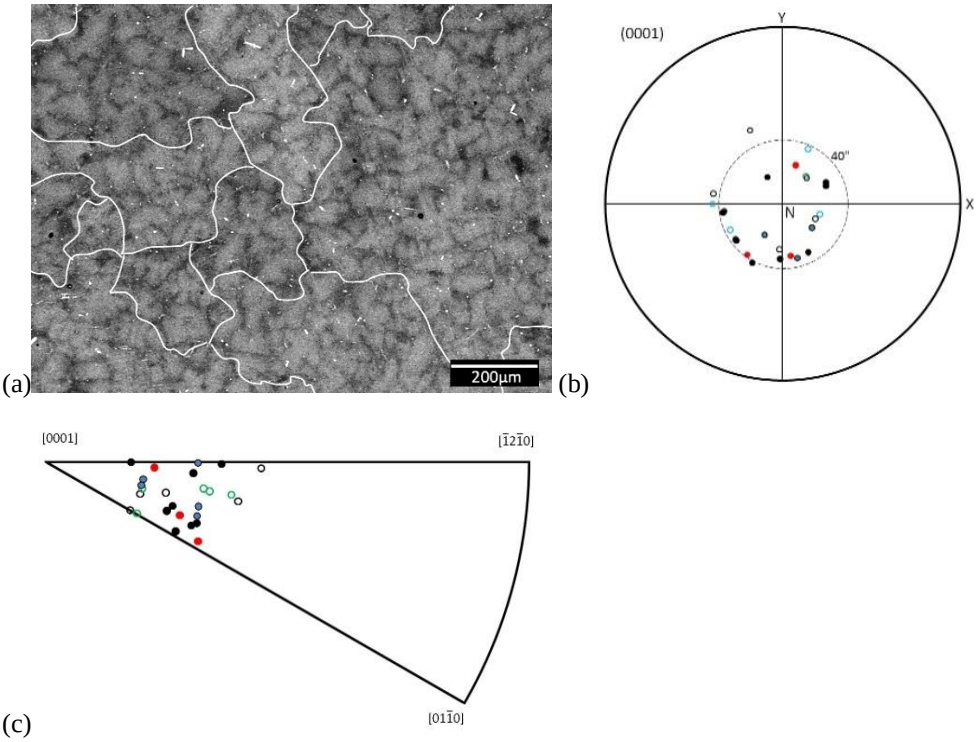

Figure 11 (a) BSE image of a cross section of the Ti48Al2Mn2Nb1B Bridgman sample in the (L+S) region with lamellar colony boundaries delineated. (b) Pole figure showing the *c*-axes of the α dendrites in (a). (c) The α dendrite growth directions derived from EBSD measurement (see Appendix I).

4. Discussion

Reflected in the title of this paper the presented work is to establish the solidification path and grain refinement mechanisms of the two alloys under the employed solidification conditions, and more importantly the relationship between them.

4.1 Solidification

Under equilibrium conditions Ti50Al-1B should solidify via the TiB_2 phase followed by the α phase according to the phase diagram[13,14]. The addition of 2% Mn and Nb is believed not to change that by a large margin. Although the actual solidification conditions, both finger ingot melting and Bridgman unidirectional solidification, were not in equilibrium, Ti50Al2Mn2Nb1B appears indeed to have solidified through the α phase, as manifested by the hexagonal dendrite morphology in Fig.1, if TiB_2 is not considered. The Ti-Al-B liquidus projections by Hymen et in 1990 [13] and Witusiewicz et al in 2009 [14] both indicate a primary TiB_2 solidification for Ti50Al-1B. The observation of homogenous distribution of sits TiB_2 particles in Ti50Al2Mn2Nb1B, without segregation into interdendritic areas as in the case of Ti48Al2Mn2Nb1B, suggests TiB_2 is the primary solidification phase, being consistent with the liquidus projections.

Ti-48Al is a hyper peritectic alloy solidifying through the reaction of $L+\beta \rightarrow \alpha+L$ under equilibrium conditions. The extent of peritectic reaction is related to the volume of the β phase before the start of peritectic reaction. The maximum β volume fraction allowed by the Ti-Al phase diagram can be calculated using a level rule as ~30% for Ti-48Al when the data reported by Witusiewicz et al are used[21]. The β volume fraction is increased with decreasing Al and it is ~90% for Ti-45Al. In Ti-48Al the solidification of the β phase would not last for long and soon be superseded by the formation of peritectic α phase. Under non-equilibrium condition the first solid metallic phase could be very different to that defined by the equilibrium phase diagram. A comprehensive study on directional peritectic solidification of Ti-(44-50)Al based on theoretical analysis was published by Su et al in 2005[22]. It revealed that with changing solidification parameters (temperature gradient G and growth rate V) not only was the phase selection changed but also the crystal growth manners. For example, at low G/V values Ti-48Al solidifies with the α phase and the α phase grows in cellular/dendritic manner. At increased G/V values the solidification turns into cellular/dendritic β and into planar α at high G/V values. Many experimental results, based on either varying cooling rate or undercooling, have demonstrated relationships between phase selection and solidification parameters in TiAl alloys[23-27].

The solidification of Ti48Al2Mn2Nb1B in both finger ingot and Bridgman sample seems to have occurred through α phase rather than the β phase, since no trace of pre-existing β phase has been evidently found through analysing Burger a variants and residual contrast caused by locally enrichment in β-stabilising element left by β to α transformation. Apart from the solidification conditions which have a strong effect on primary solidification phase selection, as mentioned above, high oxygen content and boron addition also can promote α solidification. As observed in the images shown in Figs. 8, 9 and 10a yttria particles are throughout the Bridgman samples. They were precipitated in the liquid after the primary metallic phase, which is such inferred as they are mainly located in the interdendritic areas in the images. Therefore, yttria dissolved in the molten metal before the start of solidification. The extent of oxygen contamination was investigated to details by Lapin et al and can be as

high as a few thousands wtppm[20]. In Ti-48Al alloys increasing oxygen content would push solidification pathway from peritectic to α solidification as demonstrated by Zollinger et al[28]. Boron addition is another chemistry related factor and has only been reported recently. Han et al. studied the effect of boron addition (0.2-1%) on grain refinement in 50g-button ingots of Ti48Al2Cr2Nb alloys with actual Al concentration of 47.4%[29]. It is shown that in alloys with 1%B there is no trace of pre-existing β phase whilst the segregation of β-stabilising elements left by β to α transformation is prominent in alloys with low B addition or without B. It seems that the addition of 1%B, somehow, has changed the solidification pathway from peritectic solidification to α solidification in the studied alloys. This notion is supported by the liquidus projection by Witusiewicz[14] in which increasing B changes the primary solidification phase from β to α for Ti-48Al.

The primary growth direction (PGD) of α dendrites in an α-solidifying Ti46Al0.5W0.5Si during unidirectional solidification was investigated by Li et al and it was found that the PGD varied with the growth rate when temperature gradient is at a constant[30]. With some assumptions the PGD was assigned to $<\bar{1}2\bar{1}w>$ crystalline directions (it will be close to [0001] when w is very large). The assumptions are necessary because the method used cannot take the lamellar colony rotation about its interface normal into account and such a rotation would put the PGD lying in other directions. The results from EBSD measurement from Ti48Al2Mn2Nb1B are largely scattered, as shown in Fig.11c, not particularly affiliating to $<\bar{1}2\bar{1}w>$ or $<01\bar{1}w>$. Some detailed information are given in Appendix I, showing different types of pole figures from the group of solid black data points in Figs.11b & 11c. Apparently dedicated further orientation measurement of the dendrites is needed to settle this matter.

4.2 Grain refinement

It is interesting (also surprising) to see the different grain refinement behaviour in the same alloys prepared with different methods. In finger ingots both alloys were satisfactorily grain refined whilst in the Bridgman samples the lamellar colonies are still in the form of long columns. Such a difference, combined with other observations, gives some clues to the grain refinement mechanisms. In finger ingots, regardless of Al concentration, each lamellar colony often contains one dendrite (or more dendrites in rare cases), as shown in Figs.1 and 4a but it has not been frequently identified that one dendrite was split into a few lamellar colonies through phase transformation. A plausible explanation could be that the dendrites were α-dendrites and one α-dendrite can only transform into one lamellar colony if the cooling condition is not within the Widmanstätten lamellar formation regime. A few adjacent α-dendrites with similar orientations, which is not often in ingots, could coalesce into one lamellar colony during solid phase transformation. Therefore, the lamellar colony size is governed by the α-dendrite size and its randomness in orientation. The more α-dendrites nucleate from the melt the finer the lamellar colony size. In other words, there should be no lamellar grain refinement if there is not much chance for α-dendrites to nucleate from the molten metal. This is exactly what has happened in the Bridgman samples. During unidirectional solidification process nucleation of solid from the melt is not favoured in terms

of nucleation energy barrier since solidification could proceed more easily by growth of the existing solid phase.

The observation of grain refinement in Ti48Al2Mn2Nb by boron addition can be dated back to many years ago. Guillard and Rack showed that in investment cast ϕ16mm bars the microstructure of Ti48Al2Mn2Nb was changed from columnar to fine equiaxed lamellar when B concentration was at/over 0.69%[31] and the grain refinement was indeed caused by boron addition, as proven by many studies in the following years. In other TiAl alloys, β-solidifying and hypo-peritectic solidifying, boron's grain refinement mechanisms have been established and, what is more, supported by unambiguous observations. For β-solidifying TiAl alloys grain refinement was realised through boride assisted α nucleation during $\beta \rightarrow \alpha$ solid phase transformation. Kartavykh et al published some SEM images in 2015 showing the event of solid-state germination of α phase on a curvy boride ribbon's facet and its growth into lath in a deeply etched Ti44Al5Nb2Cr1.5Zr0.4B0.07La sample[12]. In another β-solidifying alloy, Ti44Al8Nb1B, Bridgman sample, where coarse boride precipitates were found embedded in α_2 grains, a specific orientation relationship between inoculating TiB particles and the inoculated α_2 grains was revealed by EBSD analysis[17]. The inoculating effect of titanium boride on peritectic α phase was also confirmed by analysing the orientation relationship between them using EBSD in a hypo-peritectic Ti45Al2Mn2Nb1B Bridgman sample[11]. However, such direct observations of evidence have not been obtained for the grain refinement mechanisms in α-solidifying alloys, including the two in this study. The mechanisms have to be inferred.

As rationally reasoned previously the focus point of grain refinement mechanisms is at how the α dendrites were refined. Obviously, increasing α nucleation density and limiting α dendrite growth have the same effect. Sufficient amount of boride particles in the melt would increase α nucleation density though inoculation and also prevent α grain growth in solid state through Zener pinning. This scenario requires the alloys having titanium boride as the primary solidification phase. In Ti48Al2Mn2Nb1B it is unlikely the case since the boride solidified not earlier than the α phase as revealed in the microstructure of the Bridgman sample in Fig.9. As to Ti50Al2Mn2Nb1B it is unable to determine whether titanium boride is the primary solidification phase owing to the failure of the Bridgman sample, but it is possible according to the Ti-Al-B liquid projection phase diagram[14]. There are two candidate grain refinement mechanisms, depending on whether titanium boride is the primary solidification phase. In Ti48Al2Mn2Nb1B the boron-induced compositional undercooling hypothesis proposed by Cheng [32] could apply whilst in Ti50Al2Nb2Nb1B the boride inoculation, proposed by Larsen et al in 1992 and further developed by Gosslar et al later, could be employed[7,15]. To have a definite answer to the question unambiguous evidence is needed. Nonetheless, the lack of grain refinement in the Bridgman samples strongly indicates the intimate interconnection between α nucleation from the liquid and grain refinement.

Boron addition has an α-dendrite growth limiting effect in the studied alloys in this paper. The dendrites in the L+S region of the Ti48Al2Mn2Nb1B Bridgman sample are fine. They are at the order of 150μm across, similar to that of the β-dendrites in the Ti45Al2Mn2Nb1B

Bridgman sample and the later was found to be much refined comparing to the boron-free counterpart. The fine dendrite size can be attributed to the strong growth restricting factor of boron addition according Bermingham et al[33,34].

5. Conclusions

The solidification process of Ti48Al2Mn2Nb1B and Ti50Al2Mn2Nb1B has been studied using conventional solidification and unidirectional solidification techniques and the following conclusions have been reached:

1. In both Ti48Al2Mn2Nb1B and Ti50Al2Mn2Nb1B the hcp α was the first solidifying metallic phase, irrespective of the solidification techniques.

2. The growth direction of the α dendrites in Ti48Al2Mn2Nb1B during unidirectional solidification under the employed conditions deviated from the *c*-axis by 20-40°.

3. The addition of 1% boron is enough to refine the microstructures in the two alloys after conventional solidification. The lamellar colonies are refined and randomly oriented. The grain refinement was reached through enhanced α nucleation from the liquid.

4. Grain refinement did not occur in the two alloys undergoing unidirectional solidification, which can be attributed to the low opportunity of α nucleation from the liquid during solidification.

Acknowledgement – DH would like to thank Dr U Hecht for preparing the Bridgman samples.

Appendix I. Determining growth direction of α dendrites from pole figures measured from a cross section of Ti48Al2MnNb1B

The sample growth direction is at the centre of the pole figures. A dashed line is drawn from the pole of the *c*-axis through the pole figure centre and extended towards the plane trace containing the *a*-axes. In Fig.A1a the dashed line passes through an α-axis pole, and the sample growth direction lies in the line of $<\bar{1}2\bar{1}w>$. The dashed line in Fig.A1b lies in the vicinity of the black triangle which represents the pole of one of the $<01\bar{1}0>$ direction. The sample growth direction is of the type of $<01\bar{1}w>$. The pole figure in Fig.A1c is something between the two precious cases. The dashed line is between one $<\bar{1}2\bar{1}w>$ pole and one $<01\bar{1}w>$ pole. Thus, the sample growth direction in this α dendrite has an index of the type of <uvtw> (u≠v and both not zero).

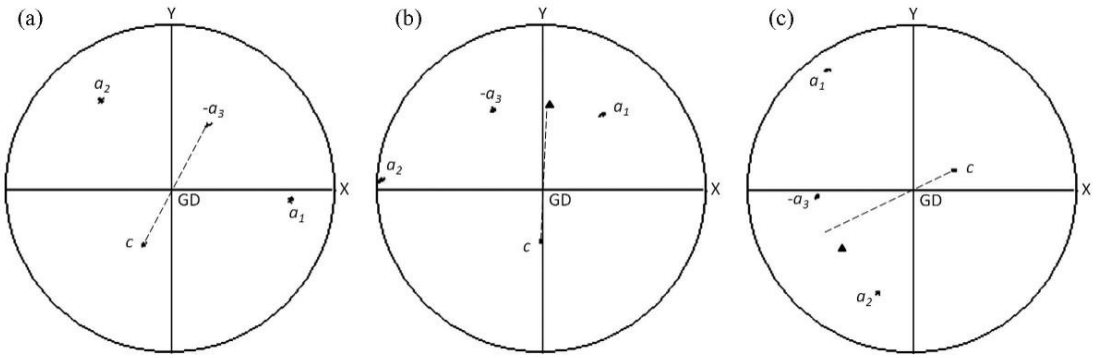

Figure A1 Pole figures of α dendrites in the (L+S) region of Ti48Al2Mn2Nb1B Bridgman sample taken from a cross section. They were used to derive the α dendrite growth direction and belong to the three types labelled as a-c.

References:

[1] Bewlay BP, Nag S, Suzuki A, Weimer MJ. TiAl alloys in commercial aircraft engines, Mater. High Temp. 2016;33:549–559.

[2] Ashraf Imam M. The 13th World Conference on Titanium (Ti-2015), JOM 2016;68(9): 2492-2501.

[3] Kim Y-W, Dimiduk DM. Progress in the understanding of gamma titanium aluminides, JOM 1991;43, August: 40-47.

[4] Kelly TJ, Weimer MJ, Austin CM, Fink PJ, Huang S-C., Method for heat treating gamma titanium aluminide alloys, US patent 1997;US005634992A.

[5] Kelly TJ, Bewlay BP, Weimer MJ, Whitacre RK. Methods for processing titanium aluminide intermetallic compositions, US patent 2013;US2013/0248061A1.

[6] Martin G, Marcillaud CJ, Mineur-Panigeon M. Heat treatment of an alloy based on titanium aluminide, US patent 2017;US2017022594A.

[7] Larsen DE, Kampe S, Christodoulo L. Effect of XD^{TM} TiB_2 volume fraction on the microstructure of a cast near-gamma titanium aluminide alloy. In: MRS Proceedings 194. San Francisco, CA; 1990. 285.

[8] Hu D. Effect of composition on grain refinement in TiAl-based alloys, Intermetallics 2001;9:1037–1043.

[9] Clemens H, Wallgram W, Kremmer S, Güther V, Otto A, Bartels A. Design of Novel β-Solidifying TiAl Alloys with Adjustable β/B2-Phase Fraction and Excellent Hot-Workability, Advanced Engineering Materials 2008;10 (8): 707-713.

[10] Imayev RM, Imayev VM, Oehring M, Appel F. Alloy design concepts for refined gamma titanium aluminide based alloys, Intermetallics 2007;15:451-460.

[11] Hu D, Yang C, Huang A, Dixon M, Hecht U. Solidification and grain refinement in Ti45Al2Mn2Nb1B, Intermetallics 2012;22:68-76.

[12] Kartavykh AV, Gorshenkov MV, Podgorny DA. Grain refinement mechanism in advanced γ-TiAl boron-alloyed structural intermetallics: The direct observation, Materials Letters 2015;142:294–298.

[13] Hyman ME, McCullough C, Levi CG, Mehrabian R. Evolution of Boride Morphologies in TiAl-B Alloys Met Trans A 1991;22A:1647.

[14] Witusiewicz VT, Bondar AA, Hecht U, Zollinger J, Artyukh LV, Ya. Velikanov T. The Al–B–Nb–Ti system V. Thermodynamic description of the ternary system Al–B–Ti, Journal of Alloys and Compounds 2009;474:86-104.

[15] Gosslar D, Günther R, Hecht U, Hartig C, Bormann R. Grain refinement of TiAl-based alloys: The role of TiB_2 crystallography and growth, Acta Materialia 2010;58:6744–6751.

[16] Hecht U, Witusiewicz V, Drevermann A, Zollinger J. Grain refinement by low boron additions in niobium-rich TiAl-based alloys, Intermetallics 2008;16:969-978.

[17] Hu D, Yang C, Huang A, Dixon M, Hecht U. Grain refinement in beta-solidifying Ti44Al8Nb1B, Intermetallics 2012;23:49-56.

[18] Yang C, Jiang H, Hu D, Huang A, Dixon M. Effect of boron concentration on phase transformation texture in as-solidified Ti44Al8NbxB, Scripta Materialia 2012;67:85–88.

[19] Hecht U, Daloz D, Lapin J, Drevermann A, Witusiewicz VT, Zollinger J. Solidification of TiAl-based alloys, MRS Proceedings 2008;1128:1128-U03-01.

[20] Lapin J, Gabalcová Z, Pelachová T. Effect of Y_2O_3 crucible on contamination of directionally solidified intermetallic Ti-46Al-8Nb alloy, Intermetallics 2011;19:396-403.

[21] Witusiewicz VT, Bondar AA, Hecht U, Rex S, Ya. Velikanov T. The Al–B–Nb–Ti system III. Thermodynamic re-evaluation of the constituent binary system Al–Ti, Journal of Alloys and Compounds 2008;465:64-77.

[22] Su Y, Liu C, Li X, Guo J, Li B, Jia J, Fu H. Microstructure selection during the directionally peritectic solidification of Ti–Al binary system, Intermetallics 2005;13:267-274.

[23] Valencia JJ, McCullough C, Levi CG, Mehrabian R. Solidification microstructure of supercooled Ti-Al alloys containing intermetallic phases, Acta metall. 1989;37:2517-2530.

[24] Nishida M, Tateyama T, Tomoshige R, Morita K, Chiha A. Electron microscopy studies of Ti - 47 at% Al powder produced by plasma rotating electrode process, Scripta Metallurgica et Materialia 1992;27:335-340.

[25] Johnson DR, Masuda Y, Inui H, Yamaguchi M. Alignment of the TiAl/Ti_3Al lamellar microstructure in TiAl alloys by directional solidification, Materials Science and Engineering 1997:A239–240:577-583.

[26] Kenel C. Leinenbach C. Influence of cooling rate on microstructure formation during rapid solidification of binary TiAl alloys, Journal of Alloys and Compounds 2015;637:242-247.

[27] Shuleshova O, Holland-Moritz D, Lindenkreuz H-G, Löser W, Büchner B. Phase selection in undercooled Ti-Al-Nb melts, Journal of Physics: Conference Series 2009;144: 012118.

[28] Zollinger J, Lapin J, Daloz D, Combeau H. Influence of oxygen on solidification behaviour of cast TiAl-based alloys, Intermetallics 2007;15:1343-1350.

[29] Han J, Xiao S, Tian J, Chen Y, Xu L, Wang X, Jia Y, Du Z, Cao S. Grain refinement by trace TiB_2 addition in conventional cast TiAl-based alloy, Materials Characterization 2015;106:112-122.

[30] Li X, Fan J, Su Y, Liu D, Guo J, Fu H. Lamellar orientation and growth direction of α phase in directionally solidified Ti-46Al-0.5W-0.5Si alloy, Intermetallics 2012;27:38-45.

[31] Guillard S, Rack HJ. Phase transformations in XD^{TM} TiB^2-reinforced near-γ Ti-48Al-2Nb-2Mn, Materials Science and Engineering, 1994;A183:181-194 .

[32] Cheng TT. The mechanism of grain refinement in TiAl alloys by boron addition - an alternative hypothesis, Intermetallics 2000;8:29-37.

[33] Bermingham MJ, McDonald SD, Nogita K, St. John DH, Dargusch MS. Effects of boron on microstructure in cast titanium alloys, Scripta Materialia 2008;59:538-541.

[34] Bermingham MJ, McDonald SD, St. John DH, Dargusch MS. Beryllium as a grain refiner in titanium alloys, Journal of Alloys and Compounds 2009;481:L20-L23.

Accepted for publication in Intermetallics. The final version can be found from the site https://www.sciencedirect.com/journal/intermetallics